Ab initio studies of ultrafast x-ray scattering of the photodissociation of iodine

Andrea Debnarova,[1] Simone Techert,[1,a)] and Stefan Schmatz[2,b)]
[1]*Max Planck Institute for Biophysical Chemistry, 37077 Göttingen, Am Faßberg 11, Germany*
[2]*Institut für Physikalische Chemie, Universität Göttingen, 37077 Göttingen, Tammannstr. 6, Germany*

(Received 22 September 2009; accepted 15 July 2010; published online 24 September 2010)

We computationally examine various aspects of the reaction dynamics of the photodissociation and recombination of molecular iodine. We use our recently proposed formalism to calculate time-dependent x-ray scattering signal changes from first principles. Different aspects of the dynamics of this prototypical reaction are studied, such as coherent and noncoherent processes, features of structural relaxation that are periodic in time versus nonperiodic dissociative processes, as well as small electron density changes caused by electronic excitation, all with respect to x-ray scattering. We can demonstrate that wide-angle x-ray scattering offers a possibility to study the changes in electron densities in nonperiodic systems, which render it a suitable technique for the investigation of chemical reactions from a structural dynamics point of view. © *2010 American Institute of Physics*. [doi:10.1063/1.3475567]

I. INTRODUCTION

The photodissociation and recombination of molecular iodine (I_2) is a simple prototypical chemical reaction, and as such it has been experimentally extensively studied.[1–5] Recently, it has become an object for the development of time-resolved pump-probe x-ray diffraction experiments, measuring the time-scales of the process with the resolution on the order of picoseconds.[6–10] In this work we focus on detailed theoretical x-ray scattering studies of relevant excited states of molecular iodine and wave packet dynamics of the motions of the nuclei during the photodissociation process. We are not concerned with the reproduction of wave packet calculation data from other groups, but rather interested in the description of the motion of the nuclei as a vehicle for our electron density computations; in other words, even classical dynamical calculations would be sufficient here.

The motivation for the choice of molecular iodine as a model system for x-ray scattering studies is straightforward because the high number of electrons results in a strong scattering signal. A second reason for choosing iodine is the simplicity and high $D_{\infty h}$ symmetry of this molecule which allows focusing on selected properties of the scattering spectra. Third, the dissociation of I_2 is an example for a chemical reaction particularly suitable for study by x-ray scattering experiments because the scattering signal dramatically changes with time up to the point when the interactions with the environment become important.

The photodissociation, triggered by a 520 nm laser pump pulse, can follow one of two paths: On the simpler first path, I_2 is excited onto a dissociative molecular potential energy curve (PEC). The second possibility is that I_2 is first excited onto a PEC with a possible bound state, but due to a PEC crossing it passes to a dissociative PEC,[11] as can be seen from Fig. 1(a) between states B and B″. The B state is the most studied excited state in I_2 as it is responsible for the visible absorption spectrum.

The nature of the photodissociation reaction renders it a good choice for time-resolved scattering experiments due to the dramatic change of the bond length, which has a strong effect on the x-ray scattering signal even when the system is studied in solution. The solvent plays an important role in the dissociation process as it hinders the diffusion of the newly created iodine pair by absorbing the kinetic energy of the separated atoms.[12] This can lead to geminate recombination of these same atoms, a process that takes places on a time-scale on the order of 10^2 picoseconds to nanoseconds. If the recombination ends with the molecule in the A or A′ state, the solvent further assists the relaxation into the ground state via an energy level crossing. The time-scale for this relaxation process strongly depends on the solvent.[2,3] Geminate recombination is a faster process in comparison to recombination of two iodine atoms not originating from the same I_2 molecule. The time-scale of both of these processes has been studied in a number of publications employing laser spectroscopy.[1–3,11,13,14]

Several theoretical studies[15–18] have been devoted to the determination of energy levels and properties of I_2. The main reason for the complicated energy level pattern of this seemingly simple molecule is the high nuclear charge of iodine leading to spin-orbit splitting of the electronic levels. The main electronic states studied in this work are depicted in Figs. 1(a) [photodissociaton] 1(b) [relaxation into the ground state]. The state denoted as B is the $^3\Pi_u(0_u^+)$ state of the visible absorption spectrum. It dissociates into $^2P_{3/2}$ and $^2P_{1/2}$ levels, while crossing repulsive or weakly bound states originating from $^2P_{3/2}$ and $^2P_{3/2}$ atomic states. This crossing results in a number of predissociation effects.[19–21]

One of the interesting implications of coherence in the case of molecular vibrational wave packets is the way in

a)Electronic mail: stecher@gwdg.de.
b)Electronic mail: sschmat@gwdg.de.

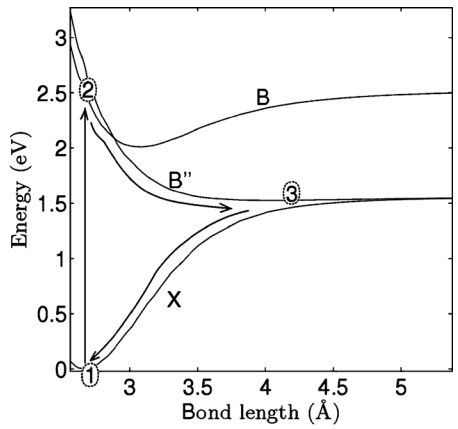

(a)

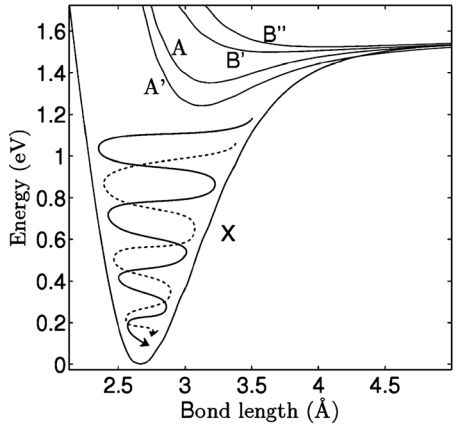

(b)

FIG. 1. (a) Potential energy curves of I_2. Schematically denoted are the photodissociation process $(1\rightarrow 2\rightarrow 3)$ and the relaxation to the ground state $(3\rightarrow 1)$. (b) Potential energy curves of I_2 with the relaxation on the ground state indicated.

which it influences the total electron density of the sample in comparison to noncoherent wave packets. Here, coherence stands for the time-evolution of the molecular wave packet in a short-time limit, before the interaction with the surrounding molecules takes place. The coherence enhances the scattering signal and consequently is a good candidate for scattering studies of the functional dependence of the electron density on time. Since the scattered x-ray intensities can be formulated as Fourier transformations (FTs) of electron densities, the time-evolution of x-ray intensities can also be described in an electron-density time-propagation scheme, presented in Sec. II and applied to an example, the photoisomerization of stilbene, in our previous work.[22]

In the following, we focus on two different aspects of x-ray scattering. First, we examine in which way small electron-density changes will influence the x-ray scattering signal. Due to the simple structure of I_2, we can directly observe how different orbital occupancies influence the scattering signal. In order to increase the predicted effect, we concentrate in respectively aligned single molecular signal changes. The second part of Sec. III complementary focuses on the effect that the coherence of the molecular wave packets has on the scattering from an ensemble of molecules. This is of particular relevance for experimental investigations in the liquid phase.

II. THEORY AND METHODOLOGY

A. FT of the electron density in terms of Gaussian-type atomic orbitals

The Debye scattering equation[23] results from classical (kinematic) x-ray scattering theory. The scattered intensity from a nonperiodic system (amorphous, liquid, or gaseous) in electron units is

$$I = \sum_m \sum_n f_m f_n \frac{\sin(kr_{mn})}{kr_{mn}}, \tag{1}$$

where f_m and f_n denote the atomic scattering factors of the mth and nth atoms in the molecule, r_{mn} is the distance between those two atoms, and $k=(4\pi \sin\theta)/\lambda$, with θ being one-half of the scattering angle. In this standard classical model, all information about chemical bonds and delocalized electron density is lost.

Ab initio quantum-chemical calculations commonly rely on Gaussian-type orbitals (GTOs) introduced by Boys[24] to model the molecular wave function. The electron density described by GTOs is also a convenient starting point for the description of scattering intensities since for these functions analytical FTs exist. For the electron density we obtain the simple Hartree–Fock or Kohn–Sham picture[22]

$$\rho(\mathbf{r}) = \sum_{i=1}^{n_{\mathrm{occ}}} b_i |\phi_i(\mathbf{r})|^2 \tag{2}$$

with occupation numbers $b_i=1,2$ and the number of occupied orbitals n_{occ}. The orbitals are expanded as

$$\phi_i(\mathbf{r}) = \sum_{\nu=1}^{N} C_{\nu i}\chi_\nu(\mathbf{r}), \tag{3}$$

where the N real basis functions χ_ν centered at $\mathbf{r}_\nu = (x_\nu, y_\nu, z_\nu)$ are defined as

$$\chi_\nu(\mathbf{r}) = \mathcal{N}_\nu (x-x_\nu)^{l_\nu}(y-y_\nu)^{m_\nu}(z-z_\nu)^{n_\nu}\exp(-\alpha_\nu(\mathbf{r}-\mathbf{r}_\nu)^2) \tag{4}$$

with normalization constant $\mathcal{N}_\nu$. Here, $l,m,n,\ldots = 0,1,2,\ldots$ denote s-, p-, d-type functions, etc. The electron density is the given by

$$\rho(\mathbf{r}) = \sum_{i=1}^{n_{\mathrm{occ}}} \sum_{\mu=1}^{N} \sum_{\nu=1}^{N} b_i C_{\mu i} C_{\nu i} \chi_\mu(\mathbf{r}) \chi_\nu(\mathbf{r}) = \sum_{i=1}^{n_{\mathrm{occ}}} \sum_{\mu=1}^{N} \sum_{\nu=1}^{N} b_i C_{\mu i} C_{\nu i} \mathcal{N}_\mu \mathcal{N}_\nu \exp\left(\frac{\alpha_\mu \alpha_\nu}{\alpha_\mu + \alpha_\nu} (\mathbf{r}_\mu - \mathbf{r}_\nu)^2 \right)$$
$$\times (x - x_\mu)^{l_\mu} (x - x_\nu)^{l_\nu} (y - y_\mu)^{m_\mu} (y - y_\nu)^{m_\nu} (z - z_\mu)^{n_\mu} (z - z_\nu)^{n_\nu} \exp(-\alpha_{\mu\nu} (\mathbf{r} - \mathbf{r}_{\mu\nu})^2)$$
$$= \sum_{i=1}^{n_{\mathrm{occ}}} \sum_{\mu=1}^{N} \sum_{\nu=1}^{N} b_i C_{\mu i} C_{\nu i} B_{\mu\nu} \prod_{\xi=x,y,z} (\xi - \xi_\mu)^{p_{\xi,\mu}} (\xi - \xi_\nu)^{p_{\xi,\nu}} \exp(-\alpha_{\mu\nu} (\xi - \xi_{\mu\nu})^2) \tag{5}$$

with

$$\alpha_{\mu\nu} = \alpha_\mu + \alpha_\nu, \tag{6}$$

$$B_{\mu\nu} = \mathcal{N}_\mu \mathcal{N}_\nu \exp\left(\frac{\alpha_\mu \alpha_\nu}{\alpha_\mu + \alpha_\nu} (\mathbf{r}_\mu - \mathbf{r}_\nu)^2 \right) \tag{7}$$

and

$$\mathbf{r}_{\mu\nu} = \frac{\alpha_\mu \mathbf{r}_\mu + \alpha_\nu \mathbf{r}_\nu}{\alpha_\mu + \alpha_\nu}. \tag{8}$$

The FT of the electron density is then written as

$$\mathcal{F}_{\mathbf{k}}\{\rho(\mathbf{r})\} = \sum_{i=1}^{n_{occ}} \sum_{\mu=1}^{N} \sum_{\nu=1}^{N} b_i C_{\mu i} C_{\nu i} B_{\mu\nu} \times$$
$$\prod_{\xi=x,y,z} \mathcal{F}_{k_\xi} \left\{ \sum_{j=0}^{p_{\xi,\mu}+p_{\xi,\nu}} c_j \xi^{p_{\xi,\mu}+p_{\xi,\nu}-j} \exp(-\alpha_{\mu\nu} (\xi - \xi_{\mu\nu})^2) \right\} \tag{9}$$

with $c_j = f(\xi_\mu, \xi_\nu)$ and $c_0 = 1$.

Generally, the FT of the polynomial expression of the density (5) has the form

$$\mathcal{F}_{\mathbf{k}}\{\rho(\mathbf{r})\} = \sum_j C_j k_x^{l_j} k_y^{m_j} k_z^{n_j} \exp(-D_j \mathbf{k}^2 - i \mathbf{k} \mathbf{r}_{\mu\nu}). \tag{10}$$

In the following, we will use this computational approach to x-ray scattering to examine detailed changes of the electron density as they occur during electronic excitations.

B. Computational details

The PECs used for wave-packet propagation calculations were taken from de Jong *et al.*[25] These PECs were calculated using two different high-level relativistic approaches for the ground and excited state calculations, respectively. The all-electron Dirac–Fock method followed by coupled cluster with single and double excitations and a perturbative triples correction [CCSD(T)] calculations were applied in the case of the ground state and so include all important relativistic effects from the outset. The excited states were calculated using an average of the configurations in the Dirac–Hartree–Fock approach followed by a complete active space configuration interaction calculation. The knowledge of the PECs is required for the simulations of the averaged wide-angle x-ray scattering signal and studies on the time-evolution involving vibrational wave-packet propagation.

In the present detailed scattering signal calculation, the iodine molecule is described using the DFT-B3LYP (Refs. 26 and 27) level of theory in conjunction with the 6-31G(d) basis set employing the Gaussian[28] program package. This would certainly be insufficient for a high-quality electronic calculation, but can easily quantify such subtle electron density changes that occur, for example, during vertical excitations.

Note, that the experiment we have referred to has been performed in the solvent CH_2Cl_2 which is known to lower the A′ potential curve of iodine [see Fig. 1(b)]. The experiment has been described in detail in Ref. 6. The scattering intensity calculations that follow these small electron density changes were performed using the program described in Ref. 22. The split-operator method[29] was used for the calculations of the wave packet dynamics in this work.

III. RESULTS AND DISCUSSION

A. The I_2 x-ray scattering spectra and excited states

A particularly interesting effect is the influence of the electronic orbital structure on the scattering pattern. To observe the effect of such details as electron density change between different excited states, one has to resort to the description of the scattering signal through the FT of detailed electron densities as it has been described in the previous section.

For a systematic build-up of the theoretical description, in the following we will concentrate on the consequences of the microscopic dynamics of iodine dissociation on the electron density changes rather than on the detailed development of a macroscopic kinetic model of structural dynamics in the liquid phase. Nonetheless, it is possible to derive the signal changes caused by the structural dynamics of single iodine molecules by integrating the single molecule density changes in the angular space coordinates. Due to the symmetry of the iodine molecule, the simulations for the various space coordinates have been performed from 0 to 180°.

We start with the total scattering map of a single iodine molecule as is depicted in Fig. 2. Here, most significant are the fast changing maxima on the k_z axis representing the I_2 bond length. The $k_z = 0$ cut of the scattering intensity spectrum appears rotationally symmetric due to the strong signal representing the core electron density confined closely to the nuclei.

One of the smallest orbital and consecutive electron-density changes of a molecule is represented by the highest

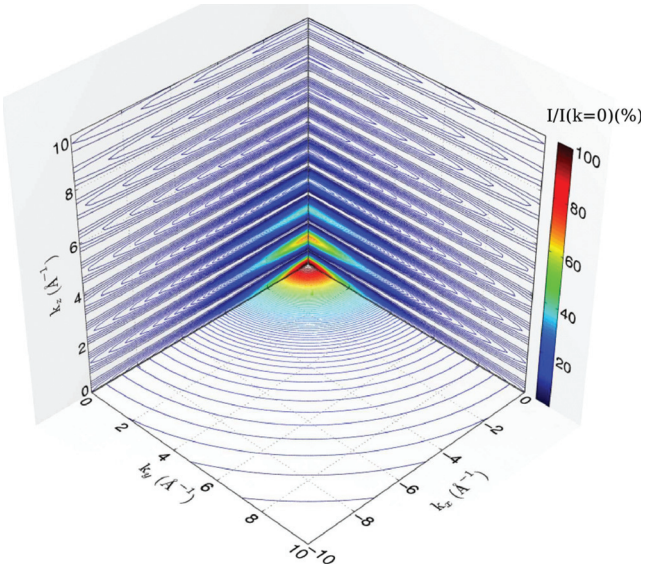

FIG. 2. Total scattering intensity of I_2. Color scale in $I/I(k=0)$ (%).

occupied molecular orbital-lowest unoccupied molecular orbital (HOMO-LUMO) excitation. In Ref. 22 we have shown that in the case of a stilbene molecule, this change causes a very small scattering signal variation of only about 0.15% in its maximum. As we will demonstrate, in the case of iodine the difference between the ground state electron density and the electron density of a vertically HOMO-LUMO excited state gives a much stronger signal in the scattering spectrum. The highest occupied (π^*) and lowest unoccupied (σ^*) electronic orbitals of iodine in the ground electronic state are depicted in Fig. 3. In Fig. 4 the intensity difference between the ground state [denoted as point 1 in Fig. 1(a)] and the HOMO-LUMO excited state [denoted as point 2 in Fig. 1(a)] is shown, which is the scattering intensity of an I_2 molecule in the lowest excited state (with the bond length of 2.73 Å) minus the scattering intensity of an I_2 molecule in its electronic ground state. Thus, this intensity difference is caused purely by the change in orbital occupancy rather than bond length change. In this way, the negative values correspond to a signal that is larger for the ground state structure while

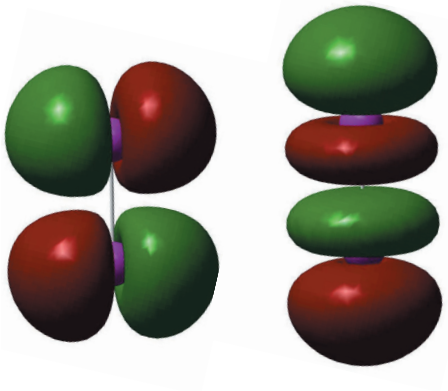

(a) (b)

FIG. 3. (a) HOMO (π_g symmetry) of I_2. (b) LUMO (σ_u symmetry) of I_2.

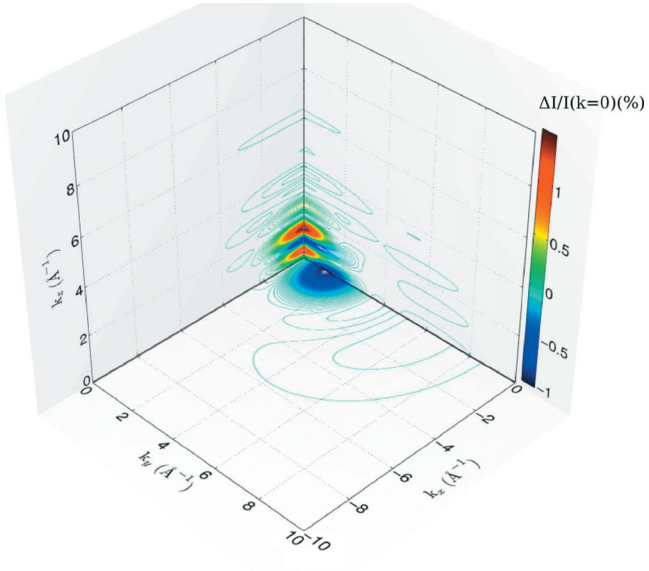

(a)

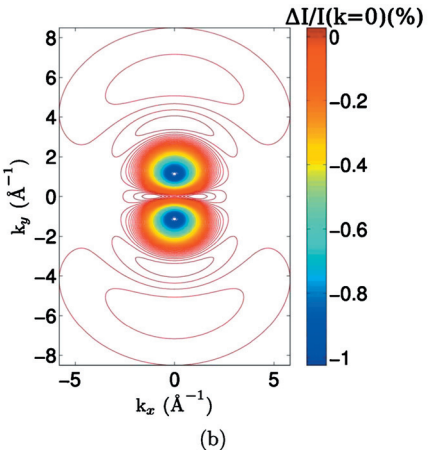

(b)

FIG. 4. I_2 scattering intensity difference in percent of $k=0$ intensity. (a) Intensity difference corresponding to the electron density change due to the HOMO-LUMO excitation from the ground state [points 1 and 2 in Fig. 1(a)]. (b) The $k_z=0$ plane of the scattering intensity. The figure resembles the first octant of k-space conserving and resembling the symmetry of iodine.

positive values correspond to a signal that is stronger in the excited state intensity spectrum. As can be seen, the symmetries of the difference scattering map correspond to the symmetries of the structural difference. The main positive maxima, about 1.5% signal change, of this intensity difference are situated on the z-axis and correspond to the redistribution of electron density from the highest occupied orbital [see Fig. 3(a)] to the lowest unoccupied orbital [Fig. 3(b)]. The HOMO is twofold degenerate and after excitation is occupied by three electrons; the LUMO is singly occupied. The total wave function is of π symmetry, and correspondingly the electron density is asymmetric in the $k_z=0$ plane. The nodal structures of the HOMO and the LUMO are also responsible for the missing electron density effect in the $k_z=0$ plane. Note that difference maps are shown and which further explains this effect because only the electron density change contributes to a visible effect.

To compare this still quite small intensity change (see the scale in Fig. 4), we now consider the dissociation of

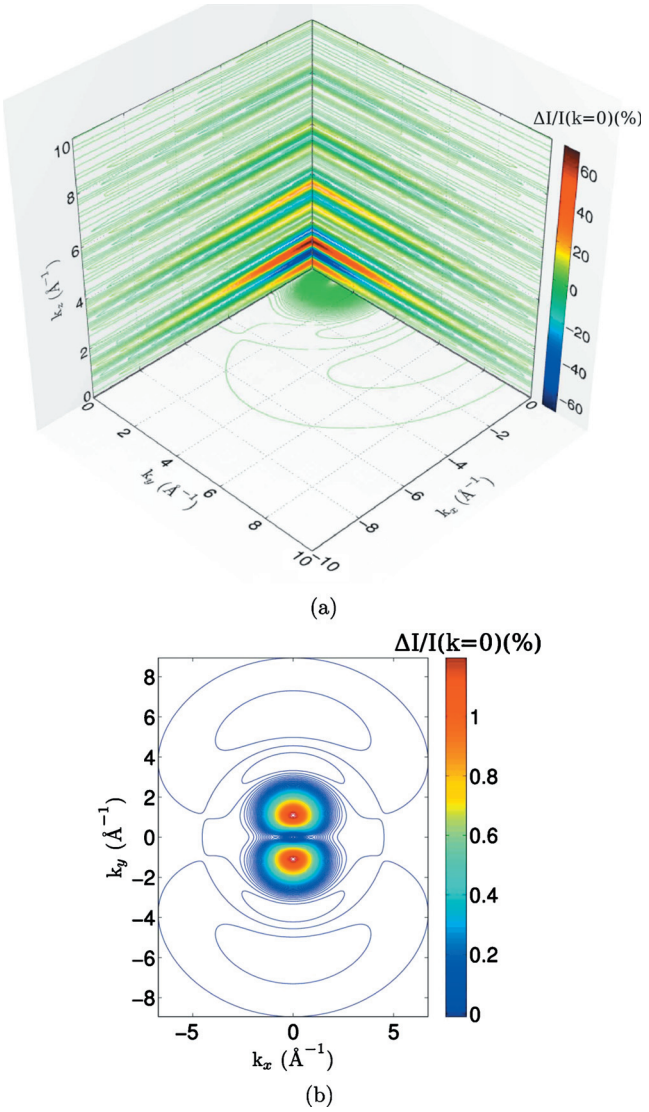

FIG. 5. I_2 scattering intensity difference in percent of $k=0$ intensity. (a) Intensity difference corresponding to the electron density difference between the HOMO-LUMO excited species with the bond length of 2.7 Å (points 2 and 1 in Fig. 1(a)] and I_2 during recombination with the bond length of 4.2 Å (point 3 in Fig. 1(a)]. (b) The $k_z=0$ plane of the scattering intensity. The figure resembles the first octant of k-space conserving and resembling the symmetry of iodine.

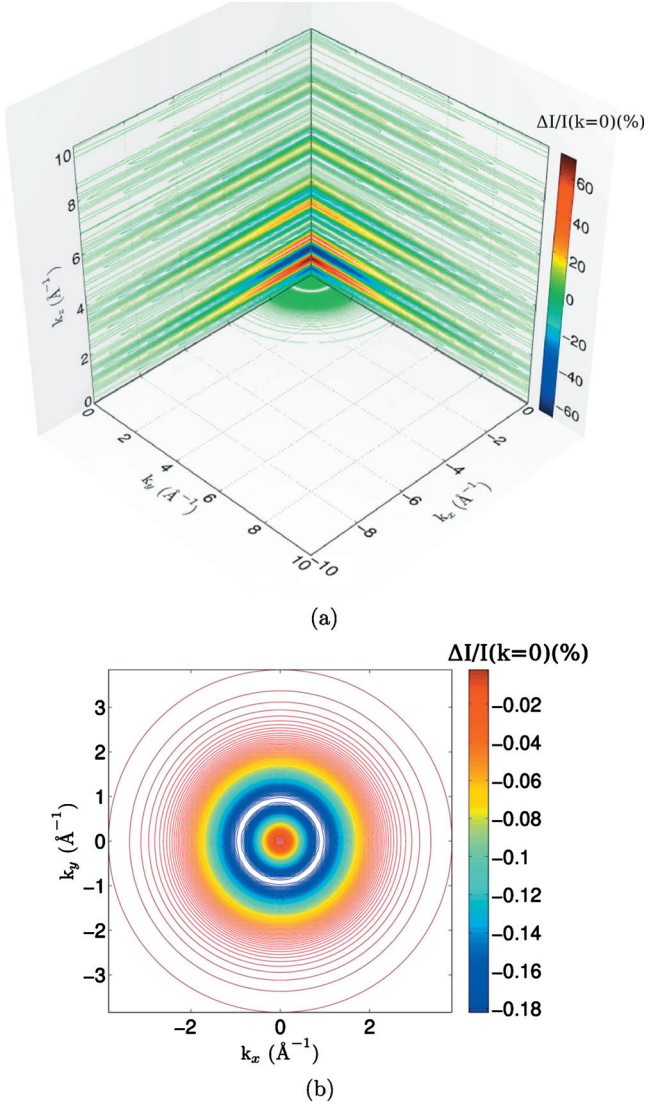

FIG. 6. I_2 scattering intensity difference in percent of $k=0$ intensity. (a) Intensity difference corresponding to the electron density change between ground states with two different bond lengths: 2.7 and 4.2 Å [points 1 and 3, respectively, with respect to point 1, in Fig. 1(a)]. (b) The $k_z=0$ plane of the scattering intensity. The figure resembles the first octant of k-space conserving and resembling the symmetry of iodine.

iodine. Figure 5 shows the intensity change when assuming a dissociation from the A′ state, the starting structure being the I_2 molecule with bond length 2.73 Å (which is the electronic ground state bond length) with the electronic structure corresponding to the HOMO-LUMO excited state. The final structure corresponds to I_2 in predissociation with a bond length of 4.2 Å with the electronic ground state orbital structure [denoted as point 3 in Fig. 1(a)]. The main maxima of the scattering signal, about 65%, here correspond to the bond-length change. However, the signal corresponding to the change in the orbital structure can well be seen on the $k_z=0$ cut, being symmetrically similar to the HOMO-LUMO electron-density scattering signal change.

A comparison of the just mentioned case with the predissociation intensity difference corresponding to two ground state (X) electron densities at different bond lengths [points 1 and 3 in Fig. 1(a)] reveals interesting results, depicted in Fig. 6. Although again the strongest signal naturally originates from the bond length change, two additional observations can be made from this picture. First, the electronic density does not undergo an asymmetric change as in the previous case, which is observable from the spherically symmetric $k_z=0$ plane of the scattering intensity difference map. However, it additionally shows another property. The picture has only negative values in the $k_z=0$ plane with two local minima of very small absolute value (about 0.18%).

In summary, on the k_z axis two effects are found: before dissociation, the change of electron density due to the HOMO-LUMO excitation leads to a 0.2% change in intensity difference, and during the dissociation process when the two iodine atoms move apart from each other integral intensity changes in the order of 60% have to be expected. Note that the two minima in Fig. 6 are very shallow and should not be attributed to the dissociation alone.

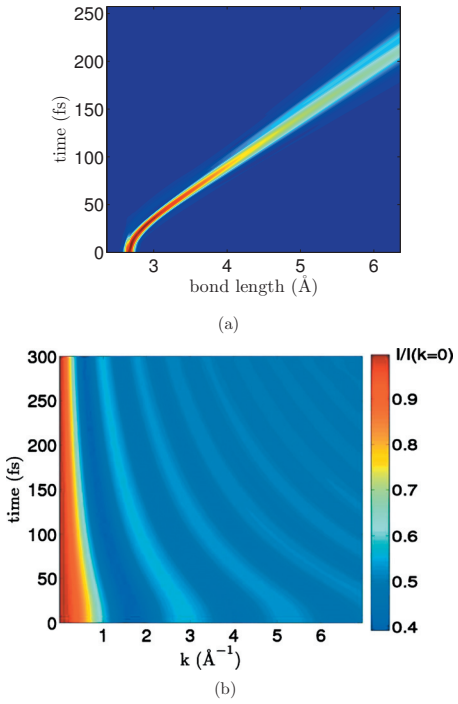

FIG. 7. Prediction of the dynamics of I_2 dissociation (a) in real space (vibrational wave packet) and (b) x-ray scattering signal (reciprocal space).

B. Observing I_2 dissociation with time-resolved x-ray scattering

The simulated system in our calculations is represented by an ensemble of iodine molecules which is randomly oriented in a well-defined angular range, corresponding to the situation in liquid samples. It should be mentioned that the experimental alignment of molecules that can be achieved will never exceed $\pm 10°$.

The ensemble in our calculation consists of 100 structures which where randomly oriented in the interval between $-10°$ and $10°$. Figure 7 displays the coherent part of the dissociation dynamics of iodine in both real and reciprocal space. It can be seen that the wave packet not only changes position with proceeding dissociation, but also loses confinement. Reflecting this behavior, the oscillations in the scattering spectrum become faster.

Figure 8 shows the effect of pulse length on the scattering signal. It can clearly be seen that in the case of dissociation, relatively long probe pulses give still quite a strong signal and time-resolved studies should be possible for up to ~ 100 fs probe pulses. Here, one has to consider the interaction between the I_2 molecule and the solvent, since the dissipation process restricts the reliable time interval of the measurement.

At long time-scales, all that can be measured with the x-ray scattering is the thermal distribution of the vibrational modes on the ground state electronic PEC as shown in Fig. 9. In the long time-scales that we refer to here, the system achieves thermal equilibrium after dissipation. The occupation of the vibrational modes depends on temperature. Figure 9 shows that although the number of occupied vibrational levels increases, the change of the scattering intensity pattern is very small, on the order of tenths of percent. As expected,

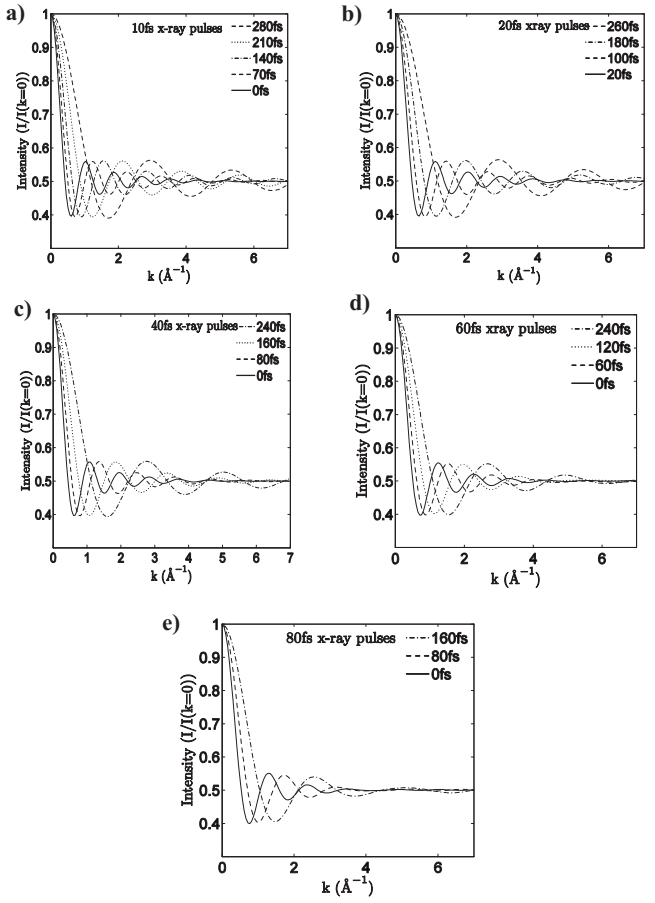

FIG. 8. Prediction of the dissociation dynamics of I_2, probed at indicated times after the photoexcitation, with x-ray pulses of finite length: (a) 10 fs FWHM of x-ray pulses, (b) 20 fs FWHM of x-ray pulses, (c) 40 fs FWHM of x-ray pulses, (d) 60 fs FWHM of x-ray pulses, and (e) 80 fs FWHM of x-ray pulses.

the higher temperatures contribute to the increase in the scattering signal in the higher k-range. The noncoherent thermal processes contribute to the diffuse signal (signal at higher k-values) and as such have only a small influence on the scattering signal of a randomly oriented molecular ensemble.

A different picture can be obtained when processes are

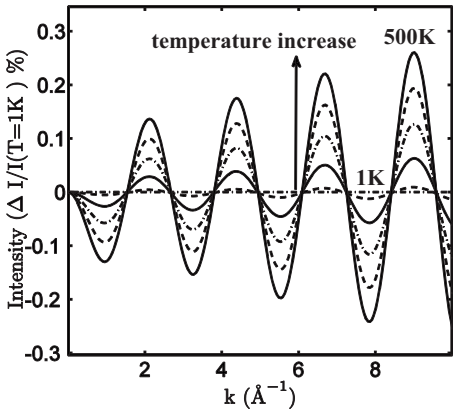

FIG. 9. Scattering intensity difference in $\Delta I/I(T=1\ \mathrm{K})$ for iodine in thermal equilibrium with a Boltzmann distribution of vibrational states at temperatures $T=1$ K to $T=500$ K. Note that reference temperature is $T=1$ K, so that the 1 K curve corresponds to the abscissa. The other curves are for $T=100$, 200, 300, 400, and 500 K.

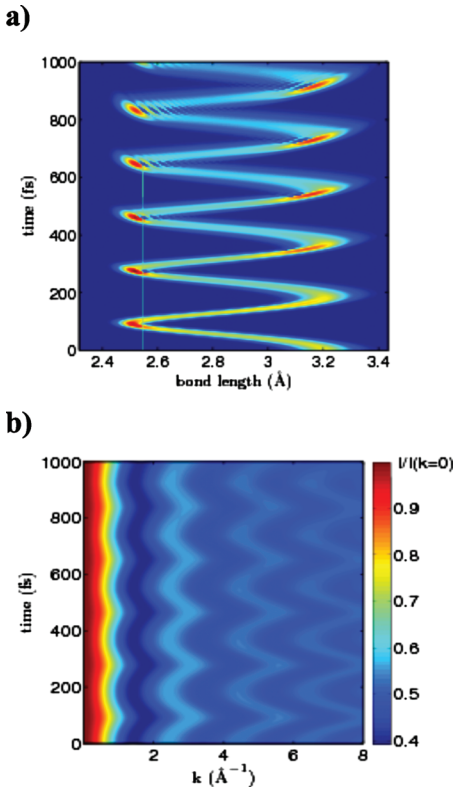

FIG. 10. Prediction of coherent relaxation of the I_2 vibrational wave packet on the ground state energy curve (a) in real space. (b) X-ray scattering signal (reciprocal space).

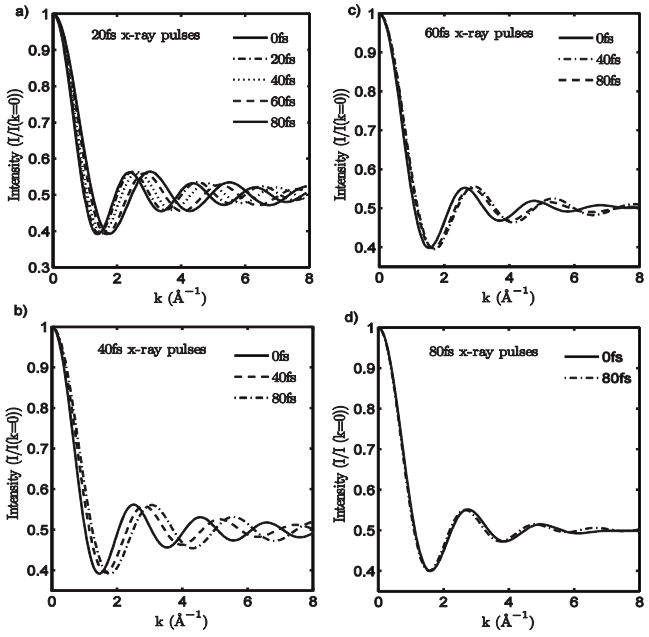

FIG. 11. Prediction of coherent relaxation of I_2 on the ground state energy curve probed with x-ray pulses of finite length: (a) 20 fs FWHM of x-ray pulses, (b) 40 fs FWHM of x-ray pulses, (c) 60 fs FWHM of x-ray pulses, and (d) 80 fs FWHM of x-ray pulses.

investigated which are confined to a small interval on the PEC by ultrafast x-ray scattering techniques. To test this kind of process we study a fictional (meaning that we have no means of starting this particular collective coherent bouncing in reality) example of coherent bouncing of the iodine molecule on the ground state PEC. The simulated dynamics in real and reciprocal space can be seen in Figs. 10(a) and 10(b). The simulations assume a 5 fs time resolution. When we study the effect of finite x-ray pulse lengths on the x-ray scattering signal of the probe pulse, for the coherent recombination case we see a picture different from the dissociation case. The first effects of the dissociation on the x-ray scattering signal are visible after 300 fs; the coherent wavepacket propagation and energy redistribution process in the iodine molecule, however, is known to be about three times faster. In the latter case, the effect of broadening of the x-ray probe pulses [their full width at half maximum (FWHMs)] strongly influences the features which can be monitored by the x-ray scattering signal in reciprocal space, as has been summarized in Fig. 11. As can be seen from Figs. 11(a)–11(d), in particular x-ray pulse lengths of 20–40 fs allow for the detection of fine scattering features such as the shift in the periodicity of the scattering function or the detection of scattering signals at higher q-values which are more smeared out for longer FWHMs of x-ray probe pulses. Thus, in the present case, very short x-ray probe pulses are of advantage for monitoring the dynamics of x-ray scattering differences of a process confined to a relatively small spatial interval on the PEC as in the present case. The calculations [see Figs. 11(d)] conclude that the simulated oscillations can only be monitored very strongly time-averaged in k-space when the x-ray probe pulse FWHM is 80 fs long, in particular since in reciprocal-space measurement the wavepacket is probed twice per oscillation period allowing to cross an interatomic distance twice per period. This probing with ~80 fs x-ray pulses corresponds to the investigation of the thermally averaged behavior of iodine molecules. Our simulations indicate that 20–40 fs x-ray pulses (FWHM) are more suitable at least for the present case. Currently, the FWHM of x-ray pulses of existing free electron laser (FEL) sources is around 20 fs.

IV. CONCLUSIONS

The modeling of the x-ray scattering of molecular iodine brought forward a number of interesting observations. First of all, even a very small electron-density change, in this case the HOMO-LUMO excitation, gives a non-negligible signal contribution when dealing with a single molecule or aligned samples. Due to the symmetry of the I_2 molecule, the small signal change that corresponds to an electron-density change caused by different orbital occupations could become observable for aligned systems. The change of the electronic state is visible on the scattering spectrum in our simulation with about 1% of signal change at $k_z, k_x = 0$ Å^{-1} in the vicinity of $k_y = 1$ Å^{-1}. It should be noted that there already exist theoretical and experimental demonstrations of such approaches (see Refs. 30 and 31 and references therein).

The notion of studying coherent molecular processes in a time-resolved x-ray scattering experiment, as for example time-resolved wide-angle x-ray scattering, is also intriguing, especially since even the control of wave-packet motion by focusing the delocalized wave-packet has been proposed[32] and experimentally proven.[33] The wave packet coherence provides a boost for the scattering signal since it provides

new equivalent structures for the constructive interference. The typical time duration of coherent processes on the order of tens to hundreds of femtoseconds, depending on the environment (gas or liquid sample), presents a limitation to the possible probe-pulse duration. At the same time, the pulse duration is limited in the same way by the necessity for high resolution in the time domain in the time-resolved experiments.

The choice of probe-pulse length also depends on the kind of the studied process, which can be either periodic or aperiodic in time. Naturally, in the case of periodic processes, such as relaxation of the wave packet on a potential energy surface after an excitation event, the probe-pulse length has to be just a fraction of the period of the process. In our test case on the relaxation of molecular iodine on the ground state curve, that has a period of about 80 fs, the probe pulse must be shorter than about 60 fs. More important is the case of aperiodic processes, as for example the iodine dissociation, where the pulse length can be longer. In our case of the first stage of the dissociation, the lengthening of the chemical bond, an event that was found to take about 300 fs, can be measured by probe pulses of up to about 80 to even 100 fs.

ACKNOWLEDGMENTS

This work was supported by DFG/SFB755 *Nanoscale Photonic Imaging*. S.T. is grateful to the Aventis Foundation and the Fonds of the Chemical Industry. A.D. thanks SFB755 for financial support. S.T. thanks the Advanced Study Group of the Max Planck Society for continuous support. S.S. is grateful to the Fonds der Chemischen Industrie for financial support.

[1] T. J. Chuang, G. W. Hoffman, and K. B. Eisenthal, Chem. Phys. Lett. **25**, 201 (1974).
[2] D. F. Kelley, N. A. Abul-Haj, and D. Jang, J. Chem. Phys. **80**, 4105 (1984).
[3] M. Berg, A. L. Harris, and C. B. Harris, J. Chem. Phys. **84**, 788 (1986).
[4] N. A. Abul-Haj and D. F. Kelley, J. Chem. Phys. **84**, 1335 (1986).
[5] A. L. Harris, J. K. Brown, and C. B. Harris, Annu. Rev. Phys. Chem. **39**, 341 (1988).
[6] R. Neutze, R. Wouts, S. Techert, A. Kirrander, J. Davidson, M. Kocsis, F. Schotte, and M. Wulff, Phys. Rev. Lett. **87**, 195508 (2001).
[7] S. Bratos, F. Mirloup, and R. Vuilleumier, J. Chem. Phys. **116**, 10615 (2002).
[8] A. Plech, M. Wulff, S. Bratos, F. Mirloup, R. Vuilleumeir, F. Schotte, and A. Anfinrud, Phys. Rev. Lett. **92**, 125505 (2004).
[9] W. Quevedo, C. Peth, G. Busse, K. Mann, and S. Techert, J. Phys. Chem. B **114**, 8593 (2010).
[10] J. Hallmann, W. Morgenroth, C. Paulmann, J. Davaasambuu, Q. Kong, M. Wulff, and S. Techert, J. Am. Chem. Soc. **131**, 15018 (2009).
[11] A. Geis, D. Block, M. Bouriau, F. Schotte, S. Techert, A. Plech, M. Wulff, and H. P. Trommsdorf, J. Lumin. **94**, 493 (2001).
[12] E. Rabinowitch and C. W. Wood, Trans. Faraday Soc. **32**, 547 (1936).
[13] D. M. P. Bado, C. Dupuy, and K. R. Wilson, J. Chem. Phys. **80**, 5531 (1984).
[14] A. L. H. M. Berg and C. B. Harris, Phys. Rev. Lett. **54**, 951 (1985).
[15] R. S. Mulliken, J. Chem. Phys. **55**, 288 (1971).
[16] G. Das and A. C. Wahl, J. Chem. Phys. **69**, 53 (1978).
[17] C. Teichteil and M. Pelissier, Chem. Phys. **180**, 1 (1994).
[18] M. Dolg, Mol. Phys. **88**, 1645 (1996).
[19] J. Vigué, M. Broyer, and J. C. Lehman, J. Chem. Phys. **42**, 949 (1981).
[20] J. Vigué, M. Broyer, and J. C. Lehman, J. Chem. Phys. **42**, 961 (1981).
[21] S. Techert and S. Schmatz, Z. Phys. Chem. **216**, 575 (2002).
[22] A. Debnarova, S. Techert, and S. Schmatz, J. Chem. Phys. **125**, 224101 (2006).
[23] B. E. Warren, *X-Ray Diffraction* (Addison-Wesley, Reading, 1969).
[24] S. F. Boys, Proc. R. Soc. London, Ser. A **258**, 402 (1960).
[25] W. A. de Jong, L. Vischer, and W. C. Nieuwpoort, J. Chem. Phys. **107**, 9046 (1997).
[26] A. Becke, J. Chem. Phys. **98**, 5648 (1993).
[27] P. J. Stephens, F. J. Devlin, C. F. Chabalowski, and M. J. Frisch, J. Phys. Chem. **98**, 11623 (1994).
[28] M. J. Frisch, G. W. Trucks, H. B. Schlegel *et al.*, GAUSSIAN 03, Revision C.02, Gaussian, Inc., Wallingford, CT, 2004.
[29] M. D. Feit, J. A. Fleck, Jr., and A. Steiger, J. Comput. Phys. **47**, 412 (1982).
[30] E. R. Peterson, C. Burth, D. A. Arms, R. W. Dunford, E. P. Kanter, B. Kassig, E. C. Landahl, S. T. Pratt, S. H. Southworth, and L. Young, Appl. Phys. Lett. **92**, 094106 (2008).
[31] J. L. Krause, R. Whitnell, K. R. Wilson, and Y. J. Yan, J. Chem. Phys. **99**, 6562 (1993).
[32] P. J. Ho and R. Santra, Phys. Rev. A **78**, 053409 (2008).
[33] B. Kohler, V. V. Yakovlev, J. Che, J. L. Krause, M. Messina, and K. R. Wilson, Phys. Rev. Lett. **74**, 3360 (1995).